Carbon 235 (2025) 120058

Contents lists available at ScienceDirect

Carbon

journal homepage: www.elsevier.com/locate/carbon

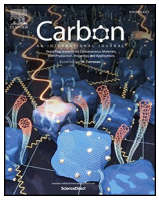

# Optimization of the carbonization process based on the evolution of microstructural components of polyacrylonitrile (PAN)-based fibers

Jiho Choi [a,1], Changbeom Jeon [b,1], Jung-Eun Lee [a], Ga-Hyeun Lee [b], Sunjae Hwang [b], Minjung Han [b], Seunghwan Lee [b], Hyeon Jung Gwak [b], Eunhye Lee [c], Jong Sung Won [c], Man Young Lee [c], Han Gi Chae [b,**], Sungho Lee [a,*]

[a] Carbon Composite Materials Research Center, Korea Institute of Science and Technology (KIST), 92 Chudong-ro, Bongdong-eup, Wanju-gun, Jeonbuk 55324, Republic of Korea
[b] Department of Materials Science and Engineering, Ulsan National Institute of Science and Technology (UNIST), Ulsan 44919, Republic of Korea
[c] Defense Materials and Energy Development Center, Agency for Defense Development, Yuseong P.O. Box 35, Daejeon 34060, Republic of Korea

ARTICLE INFO

*Keywords:*
Polyacrylonitrile (PAN)
Carbon fiber
Microstructure
SAXS
Carbonization duration
Radial heterogeneity
Optimization

ABSTRACT

This work presents a new approach for optimizing the carbonization conditions of polyacrylonitrile (PAN)-based fibers by tracing the microstructural changes during the carbonization process. Variations in the radial direction of the carbon fibers were also examined, emphasizing their correlation with temperature and duration. Changes in the outermost structure (surface) and radial heterogeneity were strongly correlated with tensile strength. Furthermore, the analysis focuses on structural changes in carbon crystallites and voids, which were analyzed using X-ray techniques, including wide-angle X-ray diffraction (WAXD) and small-angle X-ray scattering (SAXS). The size of the carbon crystallites increased exponentially with carbonization temperature and duration, forming master curves for crystallite-related properties, such as tensile modulus and void dimensions, with an identical shifting factor. These results suggest that structural changes in the radial direction critically affect mechanical properties. Based on these analyses, an optimal carbonization process was proposed, involving a duration of 2 min at 1300 °C, which resulted in a tensile strength of 3.97 GPa and a tensile modulus of 234 GPa. These findings offer a framework for optimizing the carbonization conditions to enhance the production of high-quality carbon fibers.

## 1. Introduction

Carbon fibers are regarded as next-generation materials owing to their low densities and excellent mechanical properties, leading to their continuous expansion in the global market [1,2]. Additionally, other excellent material properties such as high electrical conductivity, low thermal expansion, high-temperature tolerance, and high chemical inertness [3–7] are reasons why carbon fibers can be utilized in many different applications, including aerospace, military, automotive, civil engineering, medical applications, sporting goods, wind turbine blades, energy storage systems, and offshore drilling products [4,8–11].

Polyacrylonitrile (PAN) is a common precursor of carbon fibers because of its outstanding tensile strength [12–16]. The PAN precursor was transformed into PAN-based carbon fibers through sequential processing steps such as spinning, drawing, stabilization, carbonization, and surface treatments [17]. Among the PAN manufacturing processes, carbonization is an essential step because it involves the transition from stabilized PAN to carbon crystallites. Moreover, gas evolution occurs owing to the release of heteroatoms and structural densification during the carbonization of PAN, which significantly affects fiber properties. Therefore, optimizing the carbonization process is essential to produce high-quality PAN-based carbon fibers.

To this end, many studies have attempted to determine the optimal processing conditions for the carbonization process by controlling the initial temperature, final temperature, heating rate, and duration. First, Fitzer et al. [18] discussed the optimization of the duration and temperature of the stabilization process, as well as the temperature of the carbonization process for PAN-based fibers, focusing solely on the bulk

* Corresponding author.
** Corresponding author.
*E-mail addresses:* hgchae@unist.ac.kr (H.G. Chae), sunghol@kist.re.kr (S. Lee).
[1] These authors contributed equally to the work.

https://doi.org/10.1016/j.carbon.2025.120058
Received 3 October 2024; Received in revised form 21 January 2025; Accepted 25 January 2025
Available online 28 January 2025
0008-6223/

properties. Other studies have focused on optimizing the carbonization temperature using various experimental techniques [19,20]. Recently, modeling has been applied to optimize the carbonization process. Badrnezhad and Eslami-Farsani [21] utilized an artificial neural network fuzzy interface system to determine the optimal heat-treatment temperature. Ramezankhani et al. [22] applied the Gaussian process to predict and optimize the carbon fiber production process. Similarly, Khayyam et al. [23,24] introduced a predictive modeling technique, the convex hull method, to optimize the tensile modulus based on the tensile strength range by controlling the temperature, applied fiber tension, and nitrogen gas flow rate.

Despite the significant body of research on optimizing carbonization conditions, the effect of carbonization duration on the microstructural evolution of PAN-based fibers has not been thoroughly investigated through experimental studies. Herein, we aim to clarify how the duration of carbonization affects various structural components, including the size and orientation of carbon crystallites and voids, using X-ray techniques such as wide-angle X-ray diffraction (WAXD) and small-angle X-ray scattering (SAXS). Furthermore, we attempted to demonstrate the structural changes with particular attention to variations across the radial direction and not just the bulk properties of the carbon fibers. Specifically, we established the structure-property relationships of PAN-based carbon fibers during the carbonization process, focusing on the effect of carbonization duration. Based on our analyses of microstructural evolution, we propose optimal processing conditions for carbonization.

The remainder of this paper is structured as follows: The first section details the evolution of microvoids during carbonization across a temperature range of 400–1400 °C. The second section explores the changes in crystallite-related properties in relation to carbonization temperature and duration, presenting master curves based on shift factors calculated from the duration-temperature relationship. The third section examines the variation in tensile strength as a function of carbonization temperature and duration, with an emphasis on the primary structural factor of radial heterogeneity. Finally, by integrating the findings from the second and third sections, we propose a comprehensive approach for optimizing the carbonization process of PAN-based carbon fibers.

## 2. Materials and methods

### 2.1. Thermal treatment of PAN-based carbon fibers

A commercial PAN-based precursor fiber (Bluestar Co.) was processed using a continuous carbon fiber production line. The stabilization stage was conducted in air at temperatures of up to 270 °C for a residence time of 135 min (Iso-strain conditions). Following stabilization, low-temperature carbonization was performed under a nitrogen ($N_2$) atmosphere, reaching temperatures up to 800 °C with a duration of 2 min. High-temperature carbonization was performed to observe the microstructural evolution of the carbon fibers. To observe the effect of carbonization temperature and duration time, the strain-rates of all carbonization conditions were maintained at 15 % during low-temperature carbonization, and −3% during high-temperature carbonization, respectively. The final stage employed 35 different conditions, as listed in Table S1.

### 2.2. Characterization

The tensile properties of the carbon fibers were measured using a single-filament tensile tester (FAVIMAT+, Textechno, GmbH). Prior to testing, the linear densities of the fibers were determined using a vibroscope with a gauge length of 25.4 mm. At least 30 filaments from each specimen were subjected to tensile testing. WAXD measurements were performed at the PLS-II 6D UNIST-PAL beamline of the Pohang Accelerator Laboratory, Pohang, Republic of Korea. The energy of the X-ray was 18.986 keV and the wavelength was 0.653 Å. To obtain information about the crystalline structure in carbon fibers, the equatorial and meridional profiles were converted from 2D WAXD patterns. Each 1D profile was produced by integrating over the azimuth angle (±10°) in the respective equatorial and meridional directions along the fiber axis. The equatorial and meridional profiles were used to calculate crystal thickness and crystal size within the carbon plane, respectively. The crystal thickness of carbon (002) plane, and the crystal size within carbon plane are calculated using Scherrer's equation ($L_c = \frac{K_c\lambda}{\beta \cos\theta}$, and $L_a = \frac{K_a\lambda}{\beta \cos\theta}$), where $L_c$ is the stacking sizes perpendicular to (002) plane, $L_a$ is the crystal size within carbon plane, $\beta$ is full width at half maximum of each diffraction peak, $\theta$ is half of the peak position of each diffraction peak, $K_c$ is a constant value of 0.89, $K_a$ is a constant value of 1.84, and $\lambda$ is the X-ray wavelength, respectively [13,25–27]. Raman spectra were collected by a confocal-Raman spectrometer (Alpha 300r, WITec Co.). To investigate the radial heterogeneity of the carbon fibers, Raman spectra were obtained from three distinct radial positions: 1) the core (center of cross-sections), 2) the skin (approximately 0.7 μm from the surface toward the core), and 3) the surface. A schematic illustration of measuring the Raman spectroscopy along the radial direction is shown in Fig. S1. The Raman spectrum collected at least 7 points at each radial position. SAXS experiments were conducted using a Rigaku NANOPIX SAXS measurement system at the Research Center for Advanced Nuclear Interdisciplinary Technology, Jeonbuk National University. The X-ray photons had a wavelength of 1.54 Å and an energy of 8.04 keV. The beam diameter of SAXS experiments is 2.2 mm. The sample-to-detector distance was set at 40 cm, allowing for a q range of 0.02 $Å^{-1}$ to 0.6 $Å^{-1}$.

### 2.3. Model fitting for SAXS data

A two-dimensional SAXS speckle pattern was converted into average intensities in the meridional and equatorial directions. A nonlinear least-squares model, fitted with various numerical functions, was applied to both the vertically and horizontally averaged SAXS intensities. Quantitative information on microvoids can be acquired [12,28,29]. We utilized the form factor for a monodisperse ellipsoid with a uniform scattering length density, appropriate for the ellipsoidal-shaped microvoids inside the PAN fibers. The form factor and scattering amplitude of the ellipsoid, $P(q)$ and $f(z)$, are given by the following equations:

$$P(q) = \frac{\text{scale}}{V_{ell}}(\rho_{ell} - \rho_{solv})^2 \int_0^1 f^2 \left[ qr_b\left(1 + x^2\left(\nu^2 - 1\right)\right)^{\frac{1}{2}}\right] dx + bkg \quad (1)$$

$$f(z) = 3V_{ell}\frac{(\sin z - z\cos z)}{z^3} \quad (2)$$

where $V_{ell}$ is the volume of the ellipsoid, $\rho_{ell}$ is the scattering density of the ellipsoid, $\rho_{solv}$ scattering density of the solvent and $\nu$ is the aspect ratio of ellipsoid defined as $r_a/r_b$ ($r_a$ is the radius at the rotation axis and $r_b$ is the other radius normal to $r_a$). Model fitting for equatorial scans was conducted using the sum of two different ellipsoidal form factors for two different sizes of microvoids in the carbon fibers. When interparticle interference is not considered, the intensity of the sum of the form factors can be described as $I(Q) = n_1P_1(Q) + n_2P_2(Q) + \text{bkg}$, where $n_1$ and $P_1(Q)$ are the number density and form factor of microvoid 1, $n_2$ and $P_2(Q)$ are those of microvoid 2, and bkg is an incoherent background.

A meridional scan was performed to determine the dimensions of the carbon structures. We used the form factor for a polydisperse right circular cylinder with a uniform scattering length density [30] to describe the inner components of the pitch-derived carbon fibers, such as domains, voids, and carbon structures. The scattering amplitude of the cylinder, $F(q,\alpha)$, is given by Eq. (3),

$$F(q,\alpha) = 2V_{cyl}(\rho_{cyl} - \rho_{solv})j_0(\text{qH}\cos\alpha)\frac{J_1(\text{qr}\sin\alpha)}{(\text{qr}\sin\alpha)} \quad (3)$$

where $V_{cyl}$ is the volume of the cylinder, $\rho_{cyl}$ is the scattering density of

the cylinder, $\rho_{solv}$ is the scattering density of the solvent, $j_0(x)$ is the sine function divided by the identity function, $H$ is half the cylinder length, $\alpha$ is the angle between the cylinder axis and the scattering vector, $q$, and $J_1(x)$ is the first-order Bessel function. When the orientationally averaged cylinder form factor (integral over $\alpha$) is averaged over the Schulz distribution of the cylinder length (or radius), the size-averaged form factor is given by Eq. (4),

$$\overline{P(q)} = \frac{\text{scale}}{V_{poly}} \int_0^x f(r)\mathrm{d}r \int_0^{\pi/2} F^2(q,\alpha) sin\,\alpha d\alpha \quad (4)$$

where $V_{poly}$ is the polydisperse volume and $f(r)$ is the normalized Schulz distribution of the length (or radius). The integration of the normal cylinder form factor over the Schulz distribution of the cylinder length (or radius) results in polydispersity.

## 3. Results and discussion

### 3.1. Evolution of voids during carbonization

The carbonization of PAN-based fibers consists of four sequential steps [13]. From 400 to 600 °C, further cyclization occurs in the unstabilized structure. Then, crosslinking by dehydrogenation leads to the formation of an aromatic structure, increasing the $sp^2$ carbon structure from 600 to 800 °C [13,31]. In the third stage of the carbonization process, crosslinking between small carbon crystallites continues to increase with the release of nitrogen gas. From 1200 °C, the development of turbostratic carbon occurs. These carbonization steps include the release of gases. Therefore, it is necessary to trace the evolution of microvoids within PAN-based carbon fibers during the carbonization process.

The dimensions of the large voids located between fibrils and small voids near crystallites were calculated from the equatorial scan of the SAXS data and are shown in Fig. 1a and b, respectively.

Large voids located between fibrils show no changes during both the low (400–800 °C) and high (1000–1400 °C) temperature carbonization processes. These results indicate that cyclization and dehydrogenation during low-temperature carbonization and crystal growth during high-temperature carbonization have no effect on large voids.

Regarding the small voids located near carbon crystallites, elongation of these voids occurs between 1100 and 1400 °C. During the low-temperature carbonization process, carbon crystallites are not fully formed, resulting in small microvoids maintaining constant diameters and lengths of approximately 0.5 and 0.9 nm, respectively. Once carbon crystallites are created, their growth causes the elongation of these small voids, as shown in Fig. 1b. This occurs because nanometer-scale voids are situated between the carbon crystallites.

Notably, drastic dimensional changes in both large and small microvoids occur between 800 and 1100 °C. This is due to the release of heteroatoms and the applied shrinkage, leading to structural densification as intrinsic changes arise from the cyclized and oxidized PAN carbon crystallites.

It was possible to extract information regarding the carbon structures from the meridional scan of the SAXS data. Choi et al. [28] suggested a method for calculating the dimensions of carbon crystallites based on SAXS data with a cylindrical form factor. Here, we verified whether this analytical method is applicable to PAN-based carbon fibers. The diameters and lengths of the carbon crystallites calculated from the SAXS data were compared with the stacking sizes ($L_c$) and crystal size within carbon plane ($L_a$) of the carbon structures, as shown in Fig. 1c. The dimensions calculated from the SAXS data agreed well with those calculated from the WAXD data. SAXS is a versatile analytical technique that simultaneously provides information regarding both microvoids and the carbon structure.

### 3.2. Tensile modulus and crystal growth

In the previous section, it was explained that carbon crystallites grew during high-temperature carbonization. Specifically, the crystallite size was found to be proportional to the energy supplied to the fiber, which directly correlates with both carbonization duration and temperature. Therefore, tracing the changes in the size of the crystallites with respect to the duration and temperature of carbonization is worthwhile. As expected, the $L_c$ and $L_a$ were increased with the carbonization duration and temperature. Consequently, it was necessary to shift the curves along the temperature axis to create a master curve. To determine the shifting factor, we assumed an exponential relationship between carbonization duration and temperature, as shown in Fig. 2a.

The exponential decay function is used as follows,

$$T = \alpha \bullet e^{\left(-\frac{\Delta t}{\tau}\right)} + T_0\,, \quad (5)$$

where $T$ is carbonization temperature, $\Delta t$ is extra carbonization duration from 1 min, and $\alpha, \tau, T_0$ are the fitting parameters. A fitted curve with exponential decay was generated based on the experimental crystal size data. As a result, fitting parameters are determined as follows, $\alpha = -291$, $\tau = 13.7$, and $T_0 = 304$. The shifting factor for each curve in the plane of crystal size versus carbonization temperature was then calculated using Eq. (5), using the fitting parameters. For example, the crystal size curve of a PAN-based fiber with 3 min of high-temperature carbonization is shifted by 52.5 °C along the temperature axis. Similarly, all other curves were shifted using the shifting factor calculated using Eq. (5), and the shifted curves are shown in Fig. 2b and c. The shifted curves of the $L_c$ and $L_a$ were superimposed to form master curves.

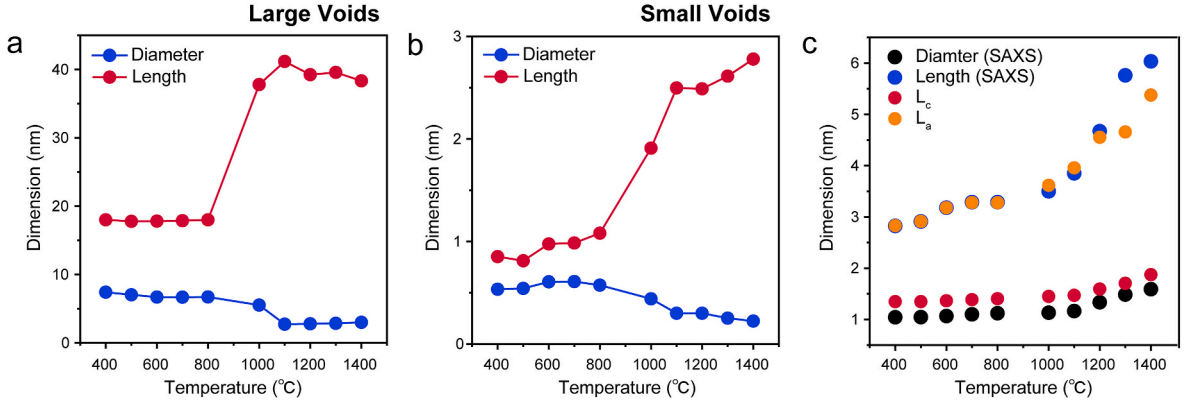


**Fig. 1.** Dimensions of fitting parameters for microvoids and carbon crystallites. (a) Large microvoids located between microfibrils. **(b)** Small microvoids located near carbon crystallites. **(c)** Comparison of carbon crystallite sizes obtained from SAXS and WAXD analyses.

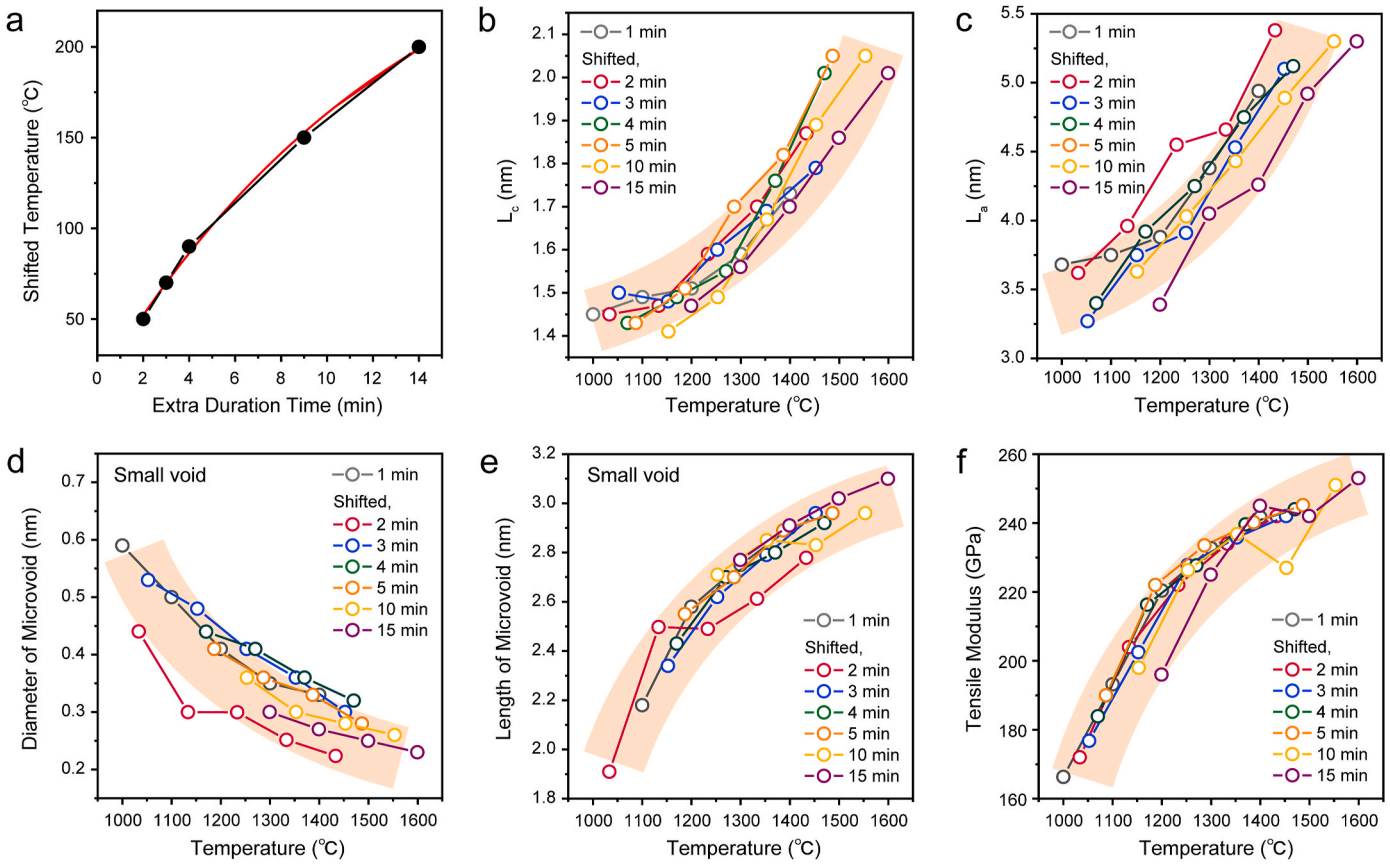


**Fig. 2.** Master curves of crystallite-related properties and tensile modulus. (a) Relationship between carbonization duration and temperature for determining shifting factors. **(b)** $L_c$. **(c)** $L_a$. **(d)** Diameter of small microvoid. **(e)** Length of small microvoid. **(f)** Tensile modulus plotted using shifting factors calculated from (a).

These master curves indicate that extending the carbonization duration has an equivalent effect to carbonization at higher temperatures, as predicted by the exponential decay function.

Several fiber properties are related to the size of the carbon crystallites. First, the size of the small microvoids located between the carbon crystallites is affected by the size of the crystallites themselves. As mentioned in the previous section, the growth of carbon crystallites induces the elongation of nanoscale microvoids. Consequently, as the length of the microvoids increases, their diameter is expected to decrease. Using the average SAXS intensities in the equatorial direction, we calculated the diameters and lengths of the small microvoids at different carbonization temperatures and durations, confirming that the results aligned with our expectations. We also applied the same shifting factor used for the crystallite size curves to the curves of the diameters and lengths of the small voids, as shown in Fig. 2d and e, respectively. Interestingly, the shifted curves also formed master curves. Notably, these shifted curves also formed master curves, further supporting the hypothesis that crystal growth leads to the elongation of nanoscale voids.

Among crystallite-related properties, the tensile modulus is a representative fiber property because it is believed to be proportional to the size of the carbon structure. Additionally, the tensile modulus is closely related to the electrical and thermal conductivities. Therefore, it is important to determine whether the same shifting factor used for crystallite size and small microvoids can be applied to the tensile modulus. We applied the same shifting factor used for the crystallite size and small microvoids to the tensile modulus curves, as shown in Fig. 2f. The shifting factor based on exponential decay, as described in Eq. (5), effectively forms a master curve for the tensile modulus. Based on the master curves shown in Fig. 2b, c, 2d, and 2f, it was concluded that a longer duration enabled the PAN fibers to achieve larger crystal sizes with more elongated nanoscale voids, leading to a higher modulus. Specifically, the relationship between carbonization duration and temperature follows the exponential decay function presented in Fig. 2a and Eq. (5), indicating that extended carbonization time is equivalent to applying higher carbonization temperatures in terms of structural evolution and fiber properties.

### 3.3. *Structural variations and their impact on tensile strength*

The tensile strength of carbon fibers is influenced by various structural factors, including surface flaws, chain ends, defects, and radial heterogeneity [6,32]. Despite numerous studies, establishing a clear correlation between these structural factors and tensile strength has been challenging. To date, bulk structural factors measured in property evaluations have not adequately accounted for radial heterogeneity, which originates from the oxidative stabilization process. Due to differences in oxygen diffusion rates between the core and surface regions during stabilization, heterogeneity develops along the radial direction of PAN-based stabilized fibers and carbon fibers [13,33,34]. Comparisons of radial heterogeneity in carbon fibers revealed that the surface regions exhibit a more oxygen-rich structure than the core regions, accelerating the development of the carbon structure during carbonization [5]. This phenomenon, known as radial heterogeneity, may significantly impact the tensile strength of carbon fibers and was investigated in detail in this study.

Raman spectra were obtained and analyzed by deconvoluting two typical carbon bands: the G band (~1580 $cm^{-1}$) and the D band (~1350 $cm^{-1}$) to investigate the radial heterogeneity of the carbon fibers [35]. Subsequently, the ratio ($I_D/I_G$) of the D band intensity ($I_D$) and the G band intensity ($I_G$) was calculated to elaborate on the effect of carbonization on carbon structures. The variation in Raman intensity was

plotted against carbonization temperature and duration for each radial position to observe radial heterogeneity, as shown in Fig. 3a–d. The core regions exhibited a less developed turbostratic structure, as evidenced by higher $I_D/I_G$ values than those in the skin regions (Fig. 3a and b), due to limited oxygen diffusion during stabilization, which typically promotes carbonization. Notably, the surface regions showed a remarkable increase in $I_D/I_G$ values beyond specific carbonization temperatures and durations (Fig. 3c). The threshold temperature decreased with increasing duration, indicating significant structural changes. This behavior is likely due to the surface regions being more susceptible to external factors during carbonization, such as applied tension, heat diffusion rate, and atmospheric conditions, which could potentially affect the mechanical properties of the carbon fibers. Furthermore, the D band (~1350 $cm^{-1}$) in carbon materials is reminiscent of defective, edge-dominant, functionalized, and $sp^3$ carbon structures, which may negatively impact the tensile strength [13,35]. Although tensile strength is influenced by various structural factors, we hypothesized that variations in $I_D/I_G$ play a critical role in this correlation.

The trend of the maximum tensile strength is shown in Fig. 3e. Notably, this trend decreases dramatically after reaching its peak, and this pattern closely resembles the trend in $I_D/I_G$ variations in the surface regions. We hypothesized that tensile fracture is primarily initiated at the surface regions, which are typical starting points for crack formation [36]. Once initiated at the surface, cracks propagate radially toward the core, ultimately leading to fracture. This suggests that the structural differences along the radial direction of the carbon fibers played distinct roles during tensile loading. However, the relative dominance of the surface versus core regions in determining mechanical properties remains unclear. In this study, we observed that the tensile strength was affected more by structural changes in the surface regions than in the core regions. Beyond the specific point where $I_D/I_G$ increased dramatically, similar trends of decreasing tensile strength were observed, as shown in Fig. 3c and e. We propose that beyond a certain level of applied energy during carbonization, the tensile strength decreases despite the independence of the $I_D/I_G$ variations in the core regions. This suggests that the surface region plays a more dominant role in crack initiation and propagation, correlating more strongly with mechanical properties than the core region.

The variation in the radial heterogeneity is shown in Fig. 3d. As mentioned above, radial heterogeneity may influence the mechanical properties of carbon fibers. To quantify this heterogeneity, we calculated the difference in $I_D/I_G$ ratios between the surface and core regions. The evolution of radial heterogeneity during carbonization can be divided into three stages: 1) an initial increase due to structural development in the surface region, 2) attainment of maximum homogeneity as $I_D/I_G$ in the surface region increases beyond specific carbonization conditions, and 3) a dramatic re-increase in heterogeneity. Interestingly, the trend in the maximum radial homogeneity closely mirrors that of the tensile strength, as shown in Fig. 3e, suggesting the critical role of radial heterogeneity in determining the mechanical properties. After the first stage, the carbon fibers appeared to reach maximum homogeneity, likely owing to an increase in the number of defective sites at the surface regions, resulting in a significant decrease in tensile strength. This observation confirms that certain carbonization conditions lead to increased radial heterogeneity beyond homogeneity, dramatically reducing the tensile strength of the carbon fibers.

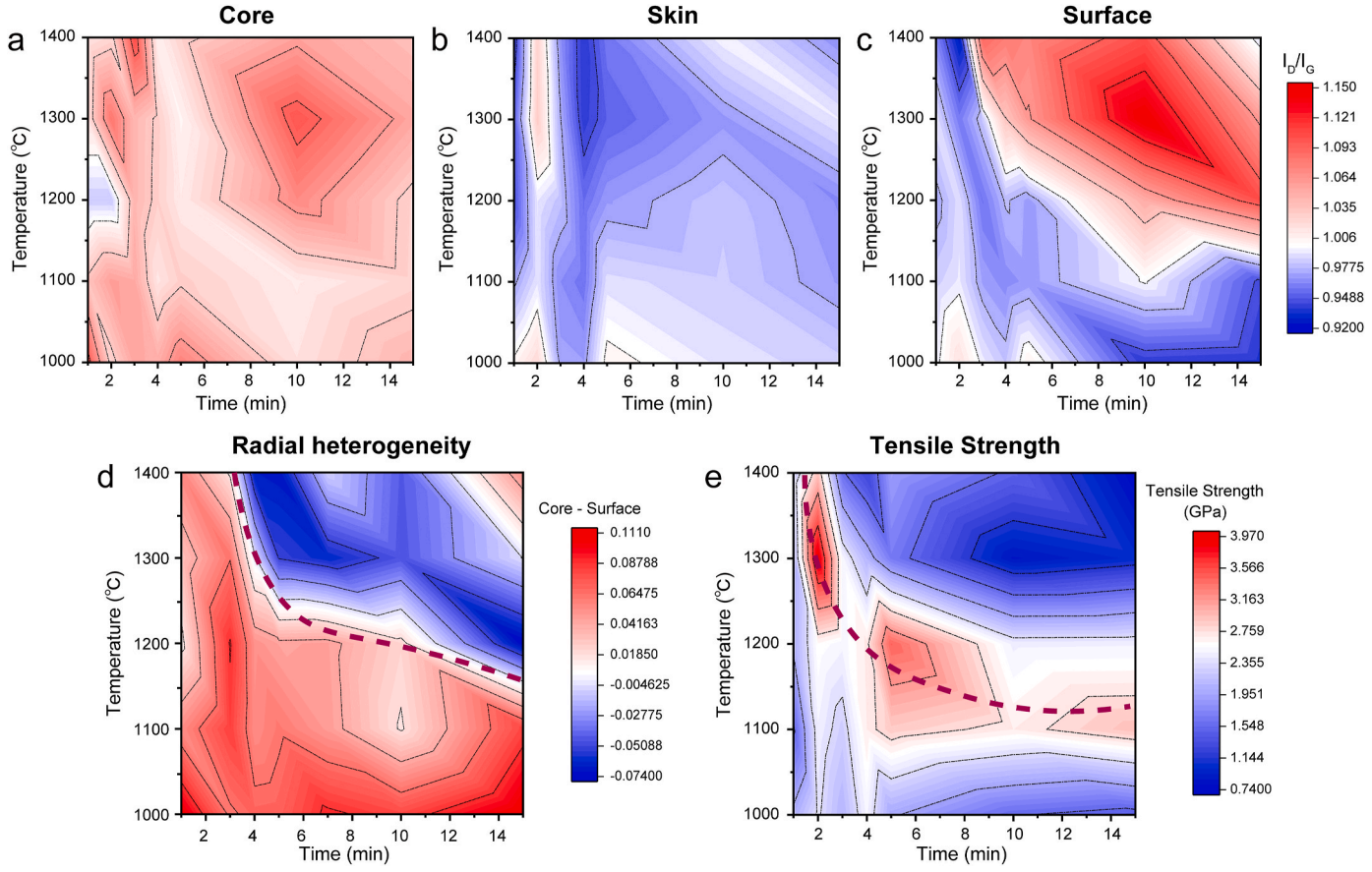


**Fig. 3.** Structural parameters and tensile strength variations with carbonization temperature and duration. (a–d) Structural parameters based on Raman spectra analysis: $I_D/I_G$ at **(a)** core regions, **(b)** skin regions, and **(c)** surface regions; **(d)** radial heterogeneity (purple dashed line indicates zero radial heterogeneity). **(e)** Tensile strength variations (purple dashed line connects the highest tensile strength for each carbonization condition). (For interpretation of the references to colour in this figure legend, the reader is referred to the Web version of this article.)

A correlation between the radial heterogeneity and tensile strength of carbon fibers was established in this study. Furthermore, the defects of carbon-based materials detected by Raman spectroscopy could be correlated with the cracks in carbon fibers on the scale of tens or hundreds of nanometers, as calculated by Griffith's equation, despite the differences in the scale of the dimensions [37]. However, this correlation between radial heterogeneity and tensile strength has not been previously reported and will be verified in more detail in future studies.

### 3.4. Optimization of the carbonization process

Previous reports indicate that the mechanical properties of carbon fibers are influenced by structural factors and processing conditions, which must be optimized to produce high-quality fibers [38,39]. Structural changes during various carbonization processes, such as temperature and duration, correlate with mechanical properties and structural factors, as discussed in Sections 3.2 and 3.3. To elucidate a clear correlation between the mechanical properties and the underlying processing factors, we employed 3D-contour mapping techniques, as plotted in Fig. 4. Among the four parameters, the tensile modulus is closely related to the carbonization temperature and duration and is plotted as z-values (Fig. 4). For instance, at a duration of 15 min and a temperature of 1400 °C, the tensile modulus reached 253 GPa, which is the maximum value among the carbon fibers studied. Additionally, as mentioned in Section 3.2, the tensile modulus was exponentially affected by the growth of carbon crystals and elongated small void structures.

In contrast to the tensile modulus, the tensile strength showed no proportional increase with temperature or duration during high-temperature carbonization, as plotted on the z-value surface (Fig. 4). The processing conditions that yield the maximum tensile strength follow an exponential trend, which is proportional to the trend in $I_D/I_G$ of the surface region or radial heterogeneity (Fig. 3). These findings suggest that the surface region plays a dominant role in influencing tensile strength and provides a straightforward approach to optimizing carbonization conditions for achieving high tensile strength in carbon fibers.

Optimization of the carbonization conditions should consider both the tensile strength and modulus [40]. Tensile strength is predominantly affected by radial structural factors such as surface region and heterogeneity but is hardly proportional to processing conditions such as temperature and duration of high-temperature carbonization. Conversely, the tensile modulus exhibited the opposite trend. The mechanical properties used in this study are listed in Table S2. We suggest optimal carbonization conditions at a duration of 2 min and a temperature of 1300 °C, balancing high tensile strength and modulus.

Such investigations could potentially contribute in several ways: 1) This is the first study to interpret the correlation between properties (tensile strength and tensile modulus) and processing conditions using a few structural factors, especially considering both bulk and specific regions of carbon fibers. 2) It is directly applicable to practical carbon fiber manufacturing because this study was conducted in a continuous heat-treatment facility. 3) In practical processing, optimal conditions can be obtained by minimizing trial and error. Overall, this work provides a foundational criterion for tailoring carbonization processes to produce high-quality carbon fibers, with enhanced tensile strength and modulus.

## 4. Conclusions

In this study, we investigated the microstructural evolution and mechanical properties of PAN-based carbon fibers under various carbonization conditions in continuous heat-treatment facilities. The size of the carbon crystallites increased exponentially with increasing temperature and duration, while the small voids between the crystallites became more elongated due to crystallite growth. We applied uniform shifting factors to create master curves for the crystallite size, void size, and tensile modulus of the carbon fibers. However, the tensile strength was correlated with the $I_D/I_G$ variations in the surface region and the radial heterogeneity of the carbon fibers. Interestingly, the tensile strength decreased significantly as the radial heterogeneity increased dramatically after reaching maximum homogeneity, independent of structural factors such as crystallites or void structures. This demonstrates the close relationship between radial heterogeneity and mechanical properties during carbonization. By optimizing the mechanical properties, we propose processing conditions that yield a tensile strength of 3.97 GPa and a tensile modulus of 234 GPa. This study provides a novel approach for optimizing the carbonization conditions in practical processes and offers an effective method for manufacturing high-quality carbon fibers based on the relationship between structure, properties, and processing analyses.

### CRediT authorship contribution statement

**Jiho Choi:** Writing – original draft, Validation, Investigation, Formal

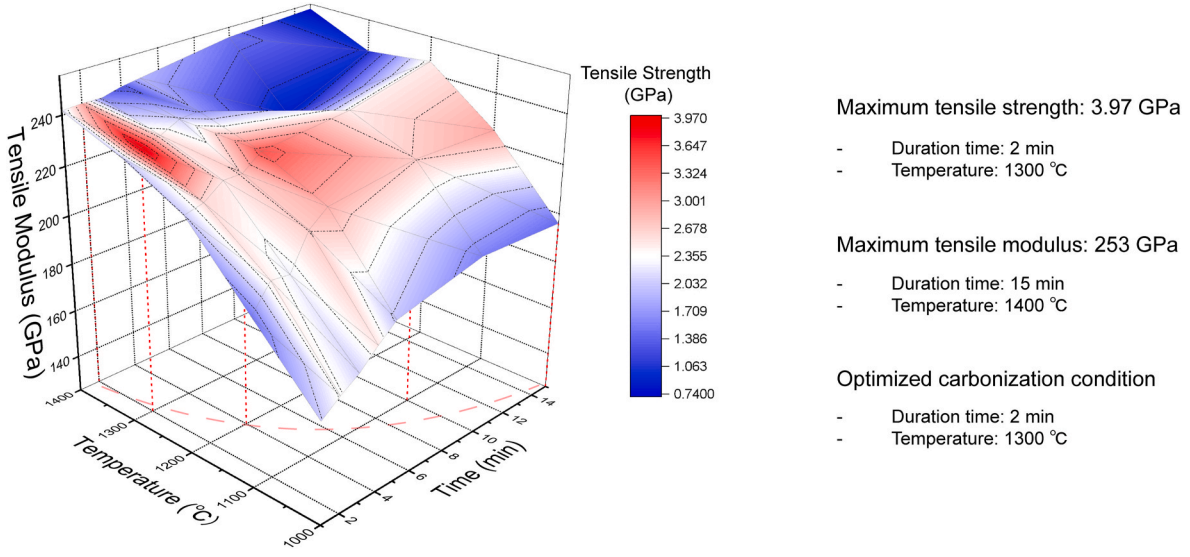


**Fig. 4.** Variations in mechanical properties of carbon fibers with carbonization temperature and duration. 3D plot showing tensile strength (surface) and tensile modulus (z-axis) as functions of carbonization temperature and duration.

analysis, Conceptualization. **Changbeom Jeon:** Writing – original draft, Validation, Methodology, Investigation, Formal analysis. **Jung-Eun Lee:** Methodology, Investigation, Formal analysis, Conceptualization. **Ga-Hyeun Lee:** Validation, Investigation, Formal analysis. **Sunjae Hwang:** Investigation, Formal analysis. **Minjung Han:** Investigation, Formal analysis. **Seunghwan Lee:** Validation, Investigation. **Hyeon Jung Gwak:** Validation, Investigation, Formal analysis. **Eunhye Lee:** Formal analysis. **Jong Sung Won:** Validation. **Man Young Lee:** Validation, Resources. **Han Gi Chae:** Writing – review & editing, Supervision, Resources, Data curation, Conceptualization. **Sungho Lee:** Writing – review & editing, Supervision, Resources, Funding acquisition, Data curation, Conceptualization.

## Declaration of competing interest

The authors declare that they have no known competing financial interests or personal relationships that could have appeared to influence the work reported in this paper.

## Acknowledgements

This work was supported by the National Research Council of Science & Technology (NST) grant by the Korea government (MSIT) (CRC23012-000) and the Materials and Components Development Program (RS-2024-00431920) funded by the Ministry of Trade, Industry & Energy, Republic of Korea. This work also was financially supported by the Institute of Civil Military Technology Cooperation funded by the Defense Acquisition Program Administration and Ministry of Trade, Industry and Energy, Republic of Korea under grant No. 22-CM-19.

## Appendix A. Supplementary data

Supplementary data to this article can be found online at https://doi.org/10.1016/j.carbon.2025.120058.

## References

[1] M. Holmes, Global carbon fibre market remains on upward trend, Reinforc Plast 58 (6) (2014) 38–45.
[2] T. Kraus, M. Kühnel, Composites-Marktbericht 2015, 2015.
[3] D.D. Edie, The effect of processing on the structure and properties of carbon fibers, Carbon 36 (4) (1998) 345–362.
[4] P. Bhatt, A. Goe, Carbon fibres: production, properties and potential use, Material Science Research India 14 (2017) 52–57.
[5] D. Choi, H.-S. Kil, S. Lee, Fabrication of low-cost carbon fibers using economical precursors and advanced processing technologies, Carbon 142 (2019) 610–649.
[6] D. Jang, M.E. Lee, J. Choi, S. Cho, S. Lee, Strategies for the production of PAN-Based carbon fibers with high tensile strength, Carbon 186 (2021).
[7] J. Choi, I. Yang, S.S. Kim, S.Y. Cho, S. Lee, Upcycling plastic waste into high value-added carbonaceous materials, Macromol. Rapid Commun. 43 (1) (2022) 2100467.
[8] Y. Singh, J. Singh, S. Sharma, T.-D. Lam, D.-N. Nguyen, Fabrication and characterization of coir/carbon-fiber reinforced epoxy based hybrid composite for helmet shells and sports-good applications: influence of fiber surface modifications on the mechanical, thermal and morphological properties, J. Mater. Res. Technol. 9 (6) (2020) 15593–15603.
[9] C.-H. Ong, S. Tsai, The Use of Carbon Fibers in Wind Turbine Blade Design: A SERI-8 Blade Example, 2000.
[10] K. Moyer, C. Meng, B. Marshall, O. Assal, J. Eaves, D. Perez, R. Karkkainen, L. Roberson, C.L. Pint, Carbon fiber reinforced structural lithium-ion battery composite: multifunctional power integration for CubeSats, Energy Storage Mater. 24 (2020) 676–681.
[11] A. Kootsookos, A.P. Mouritz, Seawater durability of glass- and carbon-polymer composites, Compos. Sci. Technol. 64 (10) (2004) 1503–1511.
[12] J.-E. Lee, Y. Chae, D. Lee, J. Choi, H. Chae, T. Kim, S. Lee, Microstructural evolution of polyacrylonitrile fibers during industry-mimicking continuous stabilization, Carbon 195 (2022).
[13] J.-E. Lee, J. Choi, D. Lee, S. Lee, H. Chae, Radial microstructure development of polyacrylonitrile (PAN)-based carbon fibers, Carbon 191 (2022).
[14] X. Guo, C. Yongxin, Z. Fan, Z. Feng, L. He, R. Liu, J. Xu, New insights into orientation distribution of high strength polyacrylonitrile-based carbon fibers with skin-core structure, Carbon 109 (2016) 444–452.
[15] X. Guo, K. Zhang, J. Cheng, H. He, L. He, J. Xu, TEM study on the inhomogeneity of oxygen diffusion distances in single polyacrylonitrile-based carbon fibers, Appl. Surf. Sci. 475 (2019) 571–576.
[16] T. You, W. Liu, Y. Sha, W. Cao, Synchrotron study on the evolution of the radial structural distribution of carbon fiber monofilaments during heat treatment process, RSC Adv. 10 (31) (2020) 18252–18258.
[17] E. Frank, L.M. Steudle, D. Ingildeev, J.M. Spörl, M.R. Buchmeiser, Carbon fibers: precursor systems, processing, structure, and properties, Angew. Chem. Int. Ed. 53 (21) (2014) 5262–5298.
[18] E. Fitzer, W. Frohs, M. Heine, Optimization of stabilization and carbonization treatment of PAN fibres and structural characterization of the resulting carbon fibres, Carbon 24 (4) (1986) 387–395.
[19] R. Shokrani Havigh, H. Mahmoudi Chenari, A comprehensive study on the effect of carbonization temperature on the physical and chemical properties of carbon fibers, Sci. Rep. 12 (1) (2022) 10704.
[20] A. Deurbergue, A. Oberlin, Stabilization and carbonization of pan-based carbon fibers as related to mechanical properties, Carbon 29 (1991) 621–628.
[21] R. Badrnezhad, R. Farsani, Modeling and differential evolution optimization of PAN carbon fiber production process, Fibers Polym. 15 (2014) 1182–1189.
[22] M. Ramezankhani, B. Crawford, H. Khayyam, M. Naebe, R. Seethaler, A. Milani, A multi-objective Gaussian process approach for optimization and prediction of carbonization process in carbon fiber production under uncertainty, Adv. Compos. Hybrid Mater. 2 (2019).
[23] H. Khayyam, S. Fakhrhoseini, J. Church, A. Milani, A. Bab-Hadiashar, R. Jazar, M. Naebe, Predictive modelling and optimization of carbon fiber mechanical properties through high temperature furnace, Appl. Therm. Eng. 125 (2017).
[24] H. Khayyam, M. Naebe, A. Bab-Hadiashar, F. Jamshidi, Q. Li, S. Atkiss, D. Buckmaster, B. Fox, Stochastic optimization models for energy management in carbonization process of carbon fiber production, Appl. Energy 158 (2015) 643–655.
[25] B. Warren, X-ray diffraction in random layer lattices, Phys. Rev. 59 (9) (1941) 693.
[26] J. Ribeiro-Soares, M. Oliveros, C. Garin, M. David, L. Martins, C. Almeida, E. Martins-Ferreira, K. Takai, T. Enoki, R. Magalhães-Paniago, Structural analysis of polycrystalline graphene systems by Raman spectroscopy, Carbon 95 (2015) 646–652.
[27] X. Ming, A. Wei, Y. Liu, L. Peng, P. Li, J. Wang, S. Liu, W. Fang, Z. Wang, H. Peng, 2D-Topology-Seeded graphitization for highly thermally conductive carbon fibers, Adv. Mater. 34 (28) (2022) 2201867.
[28] J. Choi, Y. Lee, Y. Chae, S.-S. Kim, T.-H. Kim, S. Lee, Unveiling the transformation of liquid crystalline domains into carbon crystallites during carbonization of mesophase pitch-derived fibers, Carbon 199 (2022) 288–299.
[29] J.-E. Lee, J. Choi, D. Jang, S. Lee, T.-H. Kim, S. Lee, Processing-controlled radial heterogeneous structure of carbon fibers and primary factors determining their mechanical properties, Carbon 206 (2023) 16–25.
[30] A. Guinier, G. Fournet, Small-angle scattering of X-rays, Wiley (1955).
[31] M.R. Buchmeiser, E. Muks, R. Schowner, E. Frank, U. Hageroth, S. Henzler, J. Spörl, A. Ota, R. Beyer, A. Müller, Structure evolution in all-aromatic, poly (p-phenylene-vinylene)-derived carbon fibers, Carbon 144 (2019) 659–665.
[32] H.G. Chae, S. Kumar, Making strong fibers, Science 319 (5865) (2008) 908–909.
[33] N. Hameed, J. Sharp, S. Nunna, C. Creighton, K. Magniez, P. Jyotishkumar, N. V. Salim, B. Fox, Structural transformation of polyacrylonitrile fibers during stabilization and low temperature carbonization, Polym. Degrad. Stabil. 128 (2016) 39–45.
[34] J. Choi, S.-S. Kim, Y.-S. Chung, S. Lee, Evolution of structural inhomogeneity in polyacrylonitrile fibers by oxidative stabilization, Carbon 165 (2020) 225–237.
[35] L.G. Cançado, A. Jorio, E.H.M. Ferreira, F. Stavale, C.A. Achete, R.B. Capaz, M.V. O. Moutinho, A. Lombardo, T.S. Kulmala, A.C. Ferrari, Quantifying defects in graphene via Raman spectroscopy at different excitation energies, Nano Lett. 11 (8) (2011) 3190–3196.
[36] F. Yang, G. Hu, H. He, M. Yi, Y. Ge, L. Ran, K. Peng, Effect of amorphous carbon on the tensile behavior of polyacrylonitrile (PAN)-based carbon fibers, J. Mater. Sci. 54 (11) (2019) 8800–8813.
[37] H.G. Chae, B.A. Newcomb, P.V. Gulgunje, Y. Liu, K.K. Gupta, M.G. Kamath, K. M. Lyons, S. Ghoshal, C. Pramanik, L. Giannuzzi, High strength and high modulus carbon fibers, Carbon 93 (2015) 81–87.
[38] B.A. Newcomb, Processing, structure, and properties of carbon fibers, Compos. Appl. Sci. Manuf. 91 (2016) 262–282.
[39] H. Khayyam, R.N. Jazar, S. Nunna, G. Golkarnarenji, K. Badii, S.M. Fakhrhoseini, S. Kumar, M. Naebe, PAN precursor fabrication, applications and thermal stabilization process in carbon fiber production: experimental and mathematical modelling, Prog. Mater. Sci. 107 (2020) 100575.
[40] P. Morgan, Carbon Fibers and Their Composites, CRC Press, 2005.